Chemical Engineering Journal 335 (2018) 676–684

Contents lists available at ScienceDirect

Chemical Engineering Journal

journal homepage: www.elsevier.com/locate/cej

Eu modified Cu_2O thin films: Significant enhancement in efficiency of photoelectrochemical processes through suppression of charge carrier recombination

Sanjib Shyamal[a], Paramita Hajra[a], Harahari Mandal[a], Aparajita Bera[a], Debasis Sariket[a], Ashis Kumar Satpati[b], Mikalai V. Malashchonak[c], Alexander V. Mazanik[c], Olga V. Korolik[c], Anatoly I. Kulak[d], Ekaterina V. Skorb[e,f], Arjun Maity[g,h], Eugene A. Streltsov[c], Chinmoy Bhattacharya[a,*]

[a] Indian Institute of Engineering Science & Technology, Shibpur, Howrah 711103 West Bengal, India
[b] Analytical Chemistry Division, Bhabha Atomic Research Centre, Trombay, Mumbai 400085, India
[c] Belarusian State University, Nezavisimosti Av. 4, 220030 Minsk, Belarus
[d] Institute of General and Inorganic Chemistry, National Academy of Sciences of Belarus, Surganov St. 9/1, 220072 Minsk, Belarus
[e] Harvard University, Department of Chemistry & Chemical Biology, Oxford Street, Cambridge 02138, MA, United States
[f] ITMO University, St. Petersburg 197101, Russian Federation
[g] DST/CSIR Innovation Centre, National Centre for Nanostructured Materials, Pretoria 0001, South Africa
[h] University of Johannesburg, Department of Applied Chemistry, South Africa

GRAPHICAL ABSTRACT

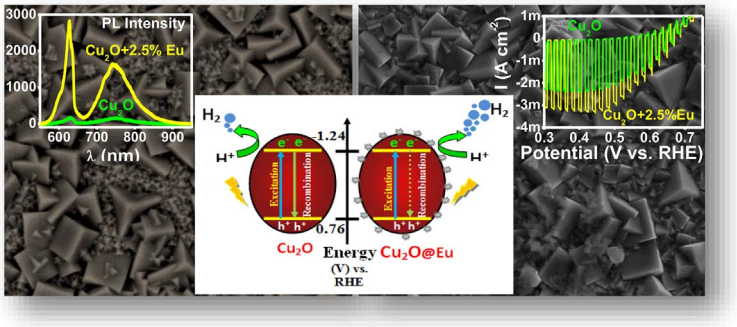

ARTICLE INFO

Keywords:
Cu_2O
Europium
Cathodic electrodeposition
Photoelectrochemical properties
Charge-carrier recombination suppression

ABSTRACT

We propose a simple way to increase incident photon-to-current conversion efficiency (IPCE, *Y*) for electrodeposited *p*-type Cu_2O films through addition of Eu(III) to the electrodeposition bath. This is the first reported enhancement of photocurrent for Cu_2O modified with a rare-earth element. Our study is based on hypothesis that a large ionic radius of Eu(III) promotes its precipitation in form of inclusions of another phase, which act as getter centers leading to purification of host material from detrimental impurities and, correspondingly, to increase in lifetime of non-equilibrium charge carriers. SEM, EDX and XRD analyses indicate that addition of Eu (III) results in some increase of Cu_2O crystallite size and growth of a secondary Eu containing phase without changing the Cu_2O lattice parameters. Electrochemical impedance spectroscopy indicates invariance of acceptor concentration and flat band potential for Eu modified films. Remarkable increase of charge carriers' lifetime,

* Corresponding author.
E-mail address: chinmoy@chem.iiests.ac.in (C. Bhattacharya).

https://doi.org/10.1016/j.cej.2017.11.004
Received 21 July 2017; Received in revised form 26 October 2017; Accepted 1 November 2017
Available online 02 November 2017
1385-8947/

which manifests in the growth of Cu_2O exciton photoluminescence (PL) intensity and PL decay constant, leads to increased IPCE for the Eu modified films. Optimization of Eu(III) concentration in the electrodeposition bath allows attaining the cathodic photocurrent as high as 3.2 mA cm^{-2} (35 mW cm^{-2} Xe lamp illumination), which is as ≈40% greater than that for the pure Cu_2O film and corresponds to $Y \approx 100\%$ at wavelength $\lambda < 450$ nm.

1. Introduction

Hydrogen evolution from renewable sources such as sunlight and water will be extremely important when the fossil-fuel supplies become depleted or when the environmental consequences of their burning are no longer acceptable. Nowadays, cuprous oxide (Cu_2O) is considered as an attractive material for the photoelectrochemical hydrogen production [1]. With a direct band gap of ≈2 eV, Cu_2O absorbs a significant part of the solar spectrum (maximal theoretical photocurrent density equals to 14.7 mA cm^{-2} under AM1.5 illumination). Availability, low toxicity, as well as favorable energy band positions for solar water splitting are obvious advantages of this semiconductor.

Since Cu_2O usually possesses *p*-type conductivity, it is of interest for solar energy primarily as a photocathode for water photoelectrolysis (hydrogen production), photoreduction of carbon dioxide (hydrocarbonate anions) [2,3], or in solid-state hetorojunction solar cells with ZnO [4] or TiO_2 [5,6]. Currently, the electrochemical deposition of Cu_2O films [1,4–41] dominates among other known chemical and physical methods (thermal and radical oxidation of copper, sputtering, SILAR, CVD, $Cu(OH)_2$ reduction, spray pyrolysis). Electrodeposition is a simple, technological, non-wasteful and inexpensive way to form thin Cu_2O films on different large-area conducting substrates (including those with a complex geometric configuration).

The most common approach to electrosynthesis of Cu_2O is based on use of aqueous solutions containing copper salt (e.g., $CuSO_4$), ligand (most often, lactate anion) and alkali (NaOH) as main components. The copper is stabilized by complexing with lactate ion, and the pH can be raised to alkaline values. Formation of Cu_2O at a cathode occurs as a result of consecutive electrochemical and chemical processes [39]. Faradaic reduction of Cu(II) complexes gives rise to formation of Cu(I) in a cathodic space. Since Cu(I) does not form stable chelate complexes with bidentate ligands, lactate complex is destroyed in an alkaline medium with formation of a Cu_2O deposit.

It was demonstrated that cuprous oxides deposited at solution pH below 7.5 are *n*-type semiconductors, while cuprous oxides deposited at a solution pH above 9.0 possess *p*-type conductivity [31]. Use of solutions without lactate anions enables one to form *n*-Cu_2O in a slightly acidic medium (pH from 5.2 to 6.4) containing acetate buffer [32]. Variation of electrodeposition conditions (solution pH, deposition potential and temperature, concentration of dopants) allows in turn formation of *p*-Cu_2O/*n*-Cu_2O homojunction solar cells [32–34].

Polycrystalline deposits with a random orientation of grains are formed on most conductive substrates. Cu_2O crystallites have a characteristic cubic shape and a typical size of several micrometers. However, Cu_2O epitaxial structures can be grown on single crystalline substrates, in particular, Au [14], InP [15,16], Si [17]. Moreover, along with electrosynthesis of polycrystalline and epitaxial films, the methods for formation of Cu_2O nanowires, nanotubes and nanorods [18–21], as well as structures with a complex morphology [22–27] are developed.

Unfortunately, practical use of the Cu_2O photoelectrodes is limited by two essential drawbacks. The first one is photocorrosion instability in aqueous solutions (Cu_2O is thermodynamically unstable both to oxidation and reduction processes [1,38]). One of the promising ways to enhance photocorrosion hardness of the Cu_2O photocathodes in hydrogen evolution processes is protection of surface by thin ZnO and TiO_2 films formed by the atomic layer deposition [1,20,29]. Additionally, electrocatalytic properties of the surface can be improved by deposition of Pt [1,29] or RuO_x [20].

The second problem related to solar energy applications of electrodeposited Cu_2O films is a rather small diffusion length of minority charge carriers (typically, a few tens of nanometers for electrons), which is much less than the depth of light penetration. As a consequence, the reported values of quantum efficiency for the photocathodes based on the electrodeposited Cu_2O films are usually significantly less than 100% (≈1% [24], ≈26% [28], ≈70% [20]) making relevant a looking for methods of charge recombination suppression. Our previous studies have demonstrated that properties of the electrodeposited Cu_2O films can be improved by variation of electrolyte composition [35,36]. Nevertheless, origins of these effects are not completely understood and require further research.

The goal of this study is to increase IPCE for electrodeposited Cu_2O films, whereas questions related to corrosion stability are outside of the scope of this work. We propose to improve the quantum efficiency by addition of europium (III) nitrate into electrodeposition solution containing copper (II) sulfate and lactic acid. Choice of Eu as a modifying additive is determined by the following reasons. Firstly, Eu^{3+} has the largest ionic radius among all lanthanides (0.109 nm), which exceeds significantly radius of Cu^+ (0.077 nm). This enables one to suppose that europium will not incorporate into the Cu_2O crystal lattice forming getter centers in the electrodeposited films and, hence, suppressing charge recombination in them. Similar approaches are applied often to improve parameters of different semiconductor materials and devices. For example, creation of internal getters in silicon wafers is widely used to increase lifetime and diffusion length of charge carriers due to bulk purification from detrimental impurities, which act as recombination centers [42,43]. Secondly, sufficiently negative standard electrode potential ($E^{0\ 3+0}_{Eu/Eu} = -1.99$ V) excludes the formation of metallic europium under cathodic electrode polarization.

There are some works devoted to the effects of Eu modifications for different semiconductors (Tables S1 and S2, Supplementary material). It has been noticed that addition of Eu improves the emission spectra of the host semiconductors, like TiO_2 [SR1-SR7], ZnO [SR8-SR11], ZnS [SR12-SR14], CdS [SR14, SR15], SiO_2 [SR16], $BaNb_2V_2O_{11}$ [SR17] etc. Among these, only some of them have reported change in photocatalytic activity of the semiconductors measured in terms of removal of pollutants [SR3], degradation of phenol [SR4, SR6], chloroform [SR7] and decoloration of dyes [SR17] and not describing the water splitting behavior. There are a rather limited number of publications dedicated to influence of rare-earths on the Cu_2O film morphology, and to the best of our knowledge, the idea to improve photoelectrochemical properties of Cu_2O films by creation of getter centers using rare-earth elements has not been suggested before.

It will be demonstrated below that an optimization of Eu(III) concentration in the electrodeposition bath enables to reach IPCE values close to 100% for the Cu_2O photocathodes.

2. Experimental section

2.1. Film preparation

2.1.1. Materials

Europium nitrate $Eu(NO_3)_3{\cdot}5H_2O$ (99.9%) was purchased from Sigma-Aldrich. Copper sulfate $CuSO_4{\cdot}5H_2O$, dipotassium hydrogen phosphate K_2HPO_4, lactic acid $CH_3CHOHCOOH$, potassium hydroxide KOH, Triton X-100 surfactant TX-100, sodium sulfate Na_2SO_4, sodium acetate CH_3COONa, acetic acid CH_3COOHwere purchased from Merck (AR grade). The FTO-coated conducting glass substrates (20 Ω/sq, Kintech Technologies, Shanghai) were cleaned by subsequent

sonication in the soap solution, ethanol and deionized water.

2.1.2. Fabrication of photoelectrodes

Cu_2O thin films were electrodeposited from the mixture of copper sulfate and europium nitrate in a basic solution. Concentration of Cu^{2+} ions in the solution was equal to 0.2 M. Europium nitrate (0, 0.5, 1.25, 2.5, 5, or 10% with respect to the Cu^{2+} concentration) was dissolved in water with the subsequent addition of dipotassium hydrogen phosphate followed by copper sulfate, lactic acid, potassium hydroxide and TX-100 surfactant. The films were deposited at a constant current density of $-0.1\ mA\ cm^{-2}$ using a DC constant current source meter (Metravi, India) in a two-electrode configuration (a Pt foil served as the counter electrode) at 30 °C for 180 min.

2.2. Film characterization

The thickness of the Cu_2O films prepared with different concentrations of Eu(III) in electrolyte was determined gravimetrically to remain within 0.5 ± 0.02 μm; the density of Cu_2O was taken in calculations equal to 6.0 g/cc [44].

The surface morphology and elemental composition of the Cu_2O films were studied through scanning electron microscopy (SEM) and energy dispersive X-ray (EDX) analysis using a LEO 1455 VP Scanning Electron Microscope. Transmission spectra of the prepared thin films were measured using a MC122 spectrophotometer (Proscan Special Instruments, Belarus). The phase composition was identified by the X-ray diffraction (XRD) analysis at a scan rate of $0.5^{\circ}\ min^{-1}$ using a Rigaku ULTIMA IV diffractometer (Bragg–Brentano geometry, Cu Kα emission). X-ray photoelectron spectra were obtained using a Thermo Scientific K-alpha spectrometer (Al K_α monochromatic X-ray source, Ar gun for surface etching).

Photoluminescence (PL) and Raman spectra were recorded at room temperature using a Nanofinder HE (LOTIS TII, Belarus – Japan) confocal spectrometer. DPSS CW laser (473 nm) was used as an excitation source. Optical power was attenuated down to 10 μW to minimize the thermal impact on the samples. Incident beam was focused on the sample surface with a 100X Olympus lens (NA = 0.95). Backscattered light was dispersed on a $600\ lines\ mm^{-1}$ diffraction grating with a spectral resolution better than $3\ cm^{-1}$ (0.1 nm in the wavelength scale) and detected using a thermostated CCD matrix with a signal acquisition time typically equal to 60 s. Calibration was performed by means of a built-in gas-discharge lamp to an accuracy better than $3\ cm^{-1}$ (0.1 nm). Lifetime of the photogenerated charge carriers was determined from PL decay kinetics at an excitation wavelength of 505 nm (Horiba, Deltadiode) with 625 emission wavelength and the spectral FWHM in continuous mode < 2 nm with the help of multifunctional time correlated single-photon counting (TCSPC) spectrophotometer (Model 1057, Fluorolog, Horiba Scientific Tech. USA).

2.3. Electrochemical impedance measurements

The electrochemical impedance measurements were carried out in pH 4.9 acetate buffer solution with 0.1 M Na_2SO_4 as supporting electrolyte with the help of Autolab-302, PG-Stat FRA-II (Metrohm, Netherlands) using the similar cell setup as detailed below. Variation of capacitance at the semiconductor-electrolyte interface (the Mott-Schottky analysis) was determined in the potential range from 0.78 to 0.28 V vs. RHE at a frequency of 1000 Hz and ac RMS amplitude of 10 mV.

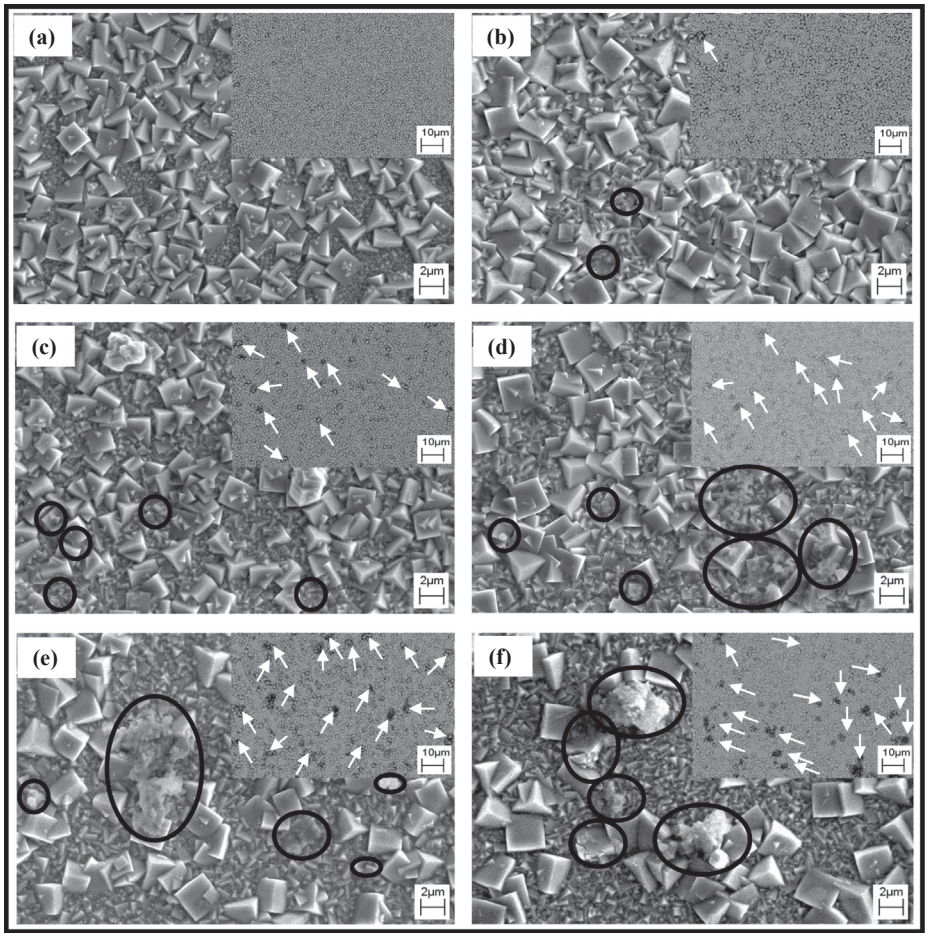

Fig. 1. SEM images of the Cu_2O films showing some precipitates (marked with black circles) along with cubic Cu_2O crystals. Images in the backscattering mode are given in insets indicating the presence of another phase (arrows). Eu(III) concentration in the electrolyte is 0% (a), 0.5% (b), 1.25% (c), 2.5% (d), 5% (e), and 10% (f).

2.4. Photoelectrochemical measurements

The photoelectrochemical properties of the prepared Cu_2O films were studied in a borosilicate glass cell with a three-electrode configuration containing a Pt rod counter and a saturated Ag/AgCl as the reference electrode. The potentials hereafter reported have been converted to the reversible hydrogen electrode (RHE). The Cu_2O working electrodes were exposed through an O-ring with a surface area of 0.27 cm^2. Linear sweep voltammetry (LSV) was carried out using a CHI-650E potentiostat within the potential range of 0.78–0.28 V vs. RHE with a scan rate of 10 mV s^{-1}. The photoresponse was measured under periodically chopped irradiation from Xe-arc lamp (Hammaan, India) as a white-light source with an incident beam intensity of 35 mW cm^{-2}, through an electrolyte containing 0.1 M Na_2SO_4 in 0.2 M sodium acetate buffer (pH 4.9). Photocurrents were also measured under illumination of 100 mW cm^{-2} using similar experimental setup to verify the effect of incident power on the PEC process.

Stability of the semiconductors undergoing photoelectrochemical H_2 evolution reaction was determined through chronoamperometry at a fixed applied potential of 0.4 V vs. RHE under constant illumination of 35 mW cm^{-2}, using similar cell configuration. The results were further verified through repeated LSV scan under periodic chopped illumination with calculation of relative deterioration of photocurrent.

PEC action spectra were measured with a high-intensity grating monochromator (spectral resolution 1 nm), a 250 W halogen lamp and a light chopper. The spectral dependences of IPCE were determined from the photocurrent and optical power of the incident monochromatic beam. The films were illuminated from the electrolyte side.

3. Results and discussion

3.1. SEM, EDX, XRD, XPS and optical characterization of Cu_2O films

SEM images demonstrate that the films are formed by cubic grains of different dimensions (Fig. 1), similar to earlier observations for the electrodeposited Cu_2O films reported by many authors. The size of the cubic grains increases to some extent with a gradual addition of Eu(III) to the electrolyte. The films deposited in presence of Eu(III) indicate some precipitates (marked with black circles) along with the main phase. These precipitates are formed possibly due to the growth of hydrated europium oxide or europium hydroxide [45] in the alkaline electrodeposition bath (pH 12–13). The SEM images obtained in the backscattering mode (insets in Fig. 1) indicate intense black spots (marked with arrows) arising from the different chemical phases as compared to the Cu_2O matrix. The pure Cu_2O films do not show such black spots, and their amount increases with a gradual rise of Eu(III) concentration in the electrodeposition bath.

EDX spectra taken under electron beam excitation of different spots on the film surface show that the “cubic” shaped particles contain primarily Cu and O without Eu (Fig. 2a) for all the films under investigation. However, for the films deposited in presence of Eu(III), EDX spectra show a definite amount of Eu (along with Cu, O from the underlaying Cu_2O grains and Sn from the FTO substrate), when secondary phase inclusions of irregular shape (marked as red circles in Fig. 1) are excited by the electron beam.

XRD patterns demonstrate peaks corresponding to the cubic Cu_2O structure (standard JCPDS file No. 05-0667) without noticeable change in their positions (Fig. 3). The absence of any peaks corresponding to Eu containing phases and retaining of “pure” Cu_2O crystallinity indicate that Eu is present in the films in amorphous forms and not being incorporated into the Cu_2O lattice. Additionally, a few peaks also appeared from the FTO substrate (standard JCPDS file No. 46-1088). The diffraction patterns demonstrate the strongest peak at $2\theta = 36.39^\circ$ corresponding to the (*hkl*) value of (1 1 1) along with the others, (1 1 0), (2 0 0), (2 2 0), (3 1 1), and (2 2 2) for all the samples. The gradual increase of Eu(III) concentration in the electrodeposition bath leads to a slight decrease in full width at half maxima (FWHM) for all peaks indicating the rise in grain size, particularly, for initial addition of Eu(III), as presented in Table 1. There is no significant modification of the film texture due to Eu(III) addition to the electrodeposition bath. One can suppose that the observed increase of grain size is related to decrease in number of electrocrystallization centers due to aggregation of defects by the europium containing inclusions.

In the Raman spectra, one can see the peaks at ≈216, ≈236, ≈300, ≈412, ≈498, ≈650, and ≈796 cm^{-1}(Fig. 4).The two most intense peaksat ≈216 and ≈650 cm^{-1} correspond to the two-phonon and one-phonon scattering processes in Cu_2O, respectively [46]. The latter band can be deconvoluted into two peaks at 632 cm^{-1} and 650 cm^{-1}, which is a consequence of TO–LO splitting for polar oscillations.

Peak fitting by Lorentz lines has demonstrated that a gradual rise of Eu(III) concentration in the bath does not affect their position and width, which is consistent with the XRD analysis and points to conservation of Cu_2O intra-grain properties. At the same time, there is a clear increasing trend in the intensity of the two-phonon band at ≈216 cm^{-1} relative to that for the one-phonon band at ≈650 cm^{-1}. Such effect, as well as an overall increase of Raman signal intensity, could be correlated to the strengthening of electron-phonon interaction in the films electrodeposited from Eu(III) containing solutions pointing to crystal quality improvement and being in a qualitative agreement with XRD and PL results (as discussed in the subsequent sections).

Raman peaks at ≈236, ≈412, ≈498, and ≈796 cm^{-1} do not correspond to symmetry-allowed one-phonon scattering processes in Cu_2O, CuO or $Eu(OH)_3$ phases [46–48]. The position of the peak at ≈300 cm^{-1} allows interpreting it as arising from one-phonon scattering in CuO [47], however, the absence of peak at ≈344 cm^{-1} inherent to CuO in the measured spectra testifies in favor of its other nature. Tentatively, all these peaks could be explained by the presence

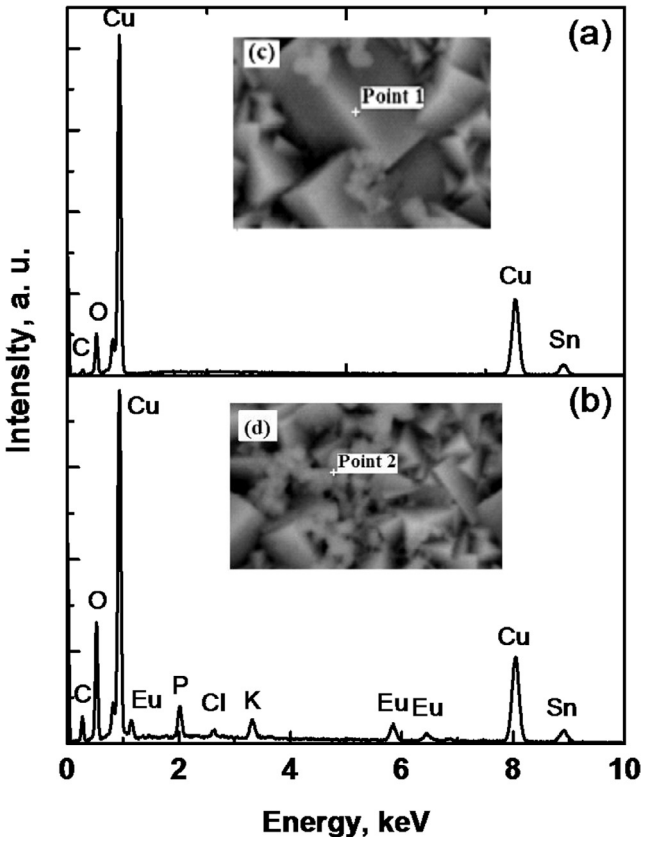

Fig. 2. EDX spectra from (a) cubic grain and (b) inclusion of irregular type for the Cu_2O film (Eu(III) concentration in the electrolyte of 2.5%). SEM images of corresponding surface regions are given in (c) and (d).

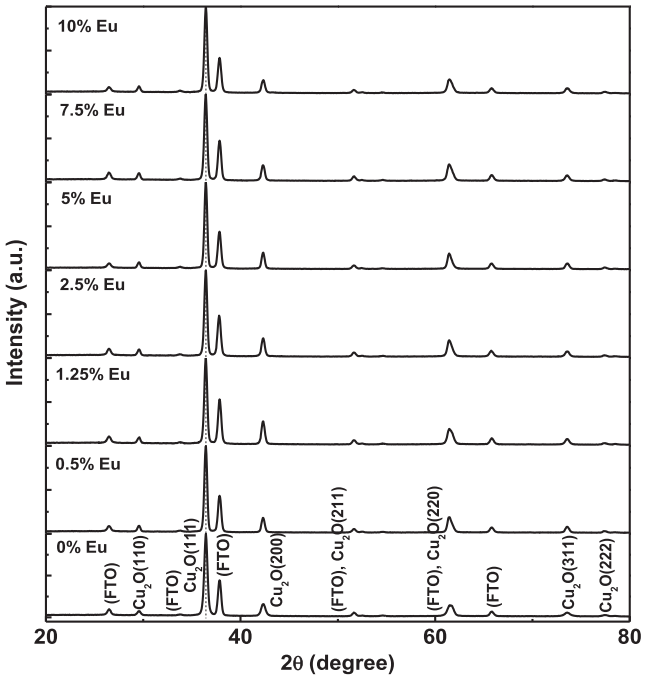

Fig. 3. XRD patterns of Cu_2O films deposited from electrolytes with different Eu(III) concentrations.

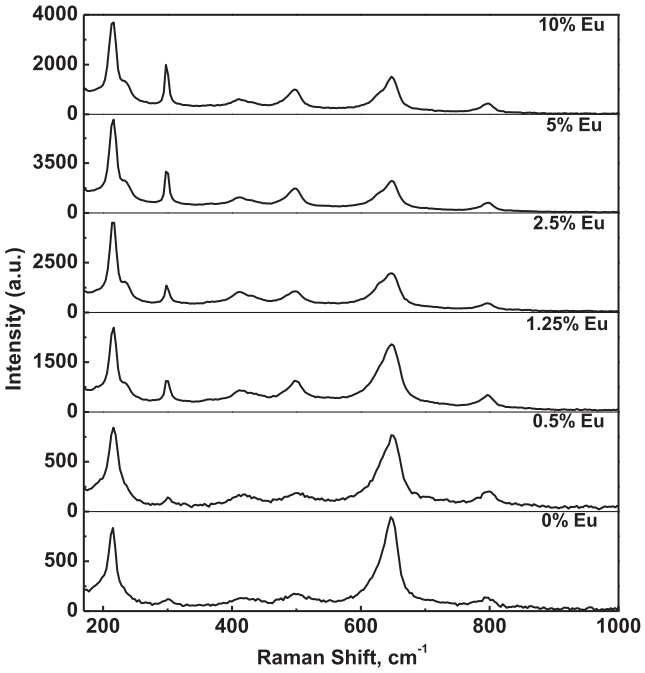

Fig. 4. Raman spectra of Cu_2O films deposited from electrolytes with different Eu(III) concentrations.

of some amorphous inclusions on the surface of the films. Meanwhile, they were observed by some researchers for Cu_2O films prepared using different techniques [49–51]. All these peaks are symmetry-forbidden in Cu_2O, and their observation points to relaxation of the symmetry-based selection rules. The most probable origin of symmetry breaking is presence of point defects (copper split vacancies) in the lattice [51]. The intensity of symmetry forbidden peaks (I_{SF}) relative to intensity of symmetry-allowed peaks (I_{SA}) inherent to Cu_2O changes from point to point for each sample, and no correlation between Eu(III) concentration in the electrodeposition bath and I_{SF}/I_{SA} ratio has been established.

XPS data show that addition of Eu(III) gives rise to increased intensity of the peaks corresponding to Cu(II) (Fig. 5a-c) [52]. Growth of Cu(II) content in the films could be explained by the known effect of coprecipitation of different hydroxides (Eu and Cu, in our case). However, in our experiments Cu(II) does not participate in photoelectrochemical processes because we used pH4.9 acetate buffer (acetic acid – sodium acetate) solutions, where Cu(II) is known to be selectively leached out [13]. As is seen from Fig. 5d, even after photoelectrochemical measurements, europium demonstrates peaks at ≈1135 and 1164 eV, which correspond to $3d_{5/2}$ and $3d_{3/2}$ electrons, respectively, and point to +3 oxidation stage [53]. This means that photocurrent increase for the Eu modified films (see below) is not related to reduction of Eu^{3+} cations.

The photoluminescence spectra of the films demonstrate two distinct bands (Fig. 6a). The high-energy band (≈625 nm) has a complicated structure and corresponds to phonon-assisted exciton recombination, whereas low-energy one (≈750 nm) is known to be related to the oxygen vacancies [54]. The fundamental possibility to observe the exciton PL at room temperature is related to extremely high exciton Rydberg energy in Cu_2O (about 0.1 eV) [55]. However, it should be noted that no exciton PL was registered in number of works devoted to Cu_2O indicating a high crystalline perfectness of our films. Fitting of exciton band with three Gauss lines shows only slight (within 2.5 nm) change of its position with Eu(III) concentration in the electrodeposition bath, which correlates with invariance of band gap energy obtained from the Tauc analysis (see below). Fig. 6b demonstrates that the introduction of Eu(III) into the electrolytic bath leads to significant increase in intrinsic PL intensity for the Cu_2O films by approximately one order of magnitude, which means suppression of non-radiative recombination processes in the matrix. TCSPC measurements (Fig. S1, Supporting material) reveal that the lifetime of the charge carriers for pure Cu_2O appears as 91 ps and increases more than two fold (up to 206 ps) for the material deposited in presence of an optimized amount (2.5%) of Eu(III) in the electrodeposition bath. The observed increase in lifetime correlates qualitatively with the grain size enlargement, as discussed in SEM analysis and is further confirmed through variation of peak width in XRD patterns (Fig. 6b). At the same time, the relative change of the grain size in the films is rather slight, whereas the PL intensity increases dramatically, suggesting the contribution of additional mechanisms to explain this effect. As it was mentioned in Introduction, a large ionic radius of Eu^{3+} reduces its

Table 1
Results of XRD analysis for Cu_2O films: FWHM of (1 1 1) peak, calculated lattice parameter and grain size values, as well as intensity ratios for different peaks with respect to that of the strongest (1 1 1) peak depending on Eu(III) concentration in electrolyte.

Eu(III) concentration in electrolyte, %	(1 1 1) peak FWHM in 2θ scale, deg	Lattice parameter, nm	Grain size, nm	$I_{(200)}/I_{(111)}$ (theor = 0.37) JCPDS file No. 05-0667	$I_{(220)}/I_{(111)}$ (theor = 0.27) JCPDS file No. 050667
0	0.353	0.4268	39	0.186	0.238
0.5	0.300		50	0.181	0.283
1.25	0.315		46	0.284	0.315
2.5	0.308		48	0.227	0.295
5	0.299		50	0.192	0.259
10	0.311		47	0.165	0.268

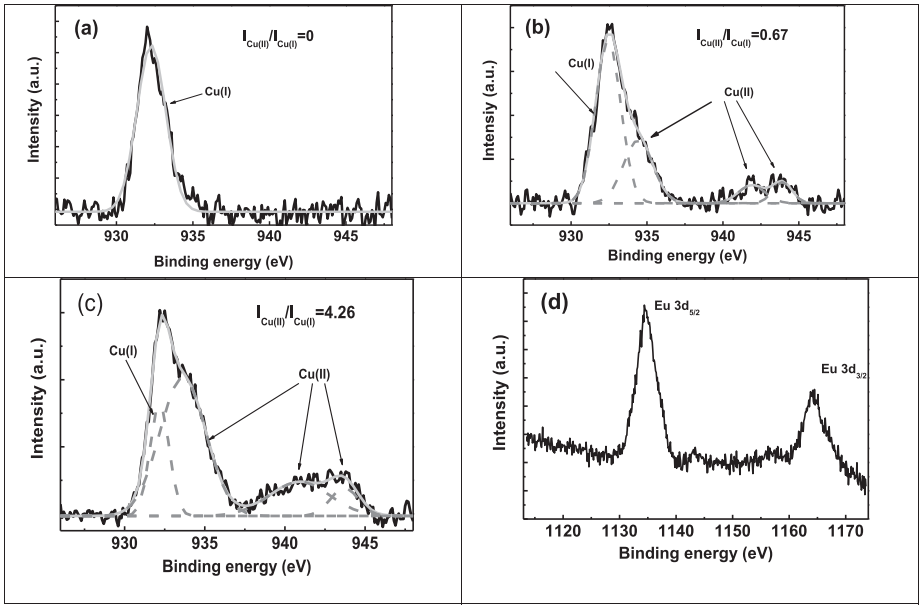

Fig. 5. XPS Cu $2p_{3/2}$ high resolution spectra for the as-grown Cu_2O films deposited from electrolytes with Eu(III) concentrationsof 0% (a), 2.5% (b), and 10% (c); Eu 3d high resolution spectrum for the Cu_2O film(Eu(III) concentration in the electrolyte of 2.5%) after photoelectrochemical measurements.

solubility in the host lattice (Cu_2O) promoting precipitation in the form of separate phase inclusions. These precipitates can act as gettering centers for detrimental impurities giving rise to purification of Cu_2O grains. Subsequently, this leads to a prominent suppression of charge carrier recombination in the Cu_2O films and thereby PL enhancement, similar to our earlier observations for chalcogenide semiconductors [56]. Formation of precipitates is well known to be favorable at grain boundaries; therefore, their passivation can be tentatively considered as an additional possible mechanism of recombination suppression.

3.2. Impedance analysis

Variation of space-charge capacitance with applied potential (Mott-Schottky plot)at a typical frequency of 1000 Hz is presented in Fig. 7. Negative slopes demonstrate *p*-type conductivity of all Cu_2O films. The acceptor concentration (N_A) and the flat-band potential (E_{fb}) were estimated from the slope and intercept at potential axis, respectively, using the Mott-Schottky equation [57] with the relative dielectric permittivity of Cu_2O taken as 7.5 [58]. From the figure it is evident that the bulk properties, i.e. the acceptor concentration ($N_A = 8.6 \times 10^{16}\,cm^{-3}$), as well as the flat band potential ($E_{fb} = 0.62$ V

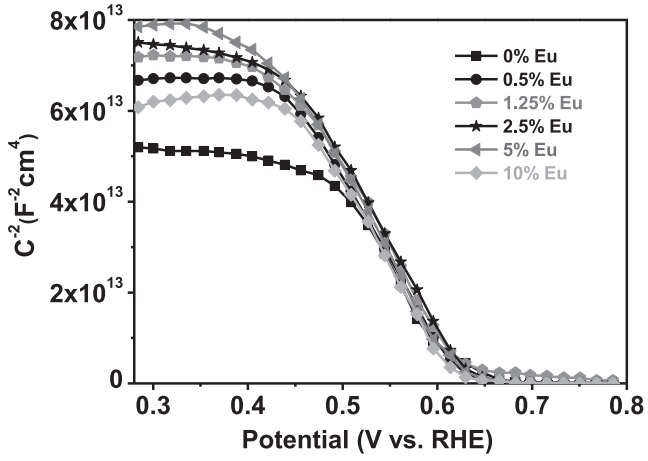

Fig. 7. Mott–Schottky plot at a typical ac frequency of 1000 Hz for Cu_2O films deposited from electrolytes with different Eu(III) concentrations.

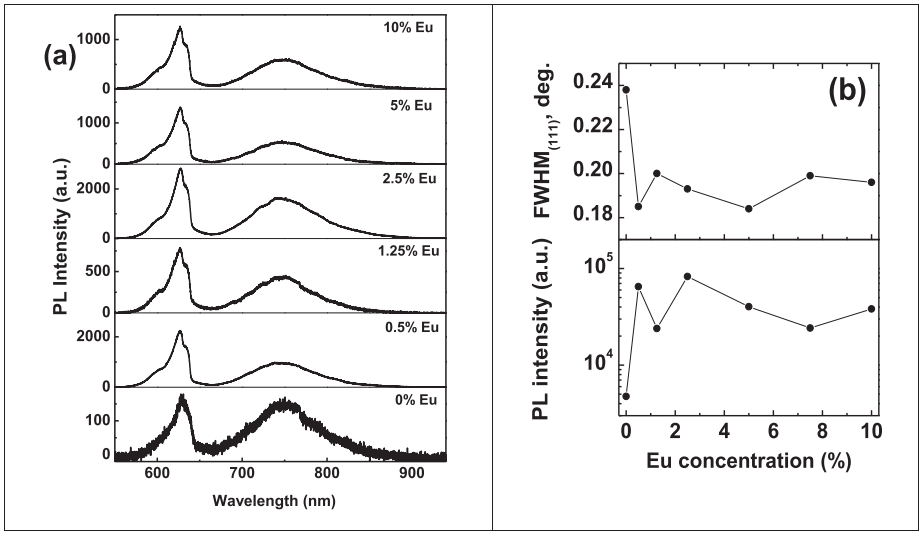

Fig. 6. (a) PL spectra of Cu_2O films deposited from electrolytes with different Eu(III) concentrations; (b) FWHM of Cu_2O (1 1 1) reflex and wavelength integrated intensity of Cu_2O exciton PL band vs. Eu(III) concentration in electrolyte.

vs. RHE) remain almost constant for all the films in depending of Eu(III) concentrations in the electrodeposition bath. Constancy of N_A points to absence of europium induced ion doping effect. The position of the conduction band (–1.74 V vs. RHE) as estimated from the experimental N_A, E_{fb} data and E_g value for direct allowed optical transitions (see below) is at more cathodic potential side compared to that required for reduction of H_2O indicating applicability of the present semiconductor for cathodic hydrogen evolution. Note that the calculated N_A value is overestimated to some extent because the geometrical surface area used in the Mott-Schottky equation is smaller as compared to the real surface area of the "Cu_2O-electrolyte" interface (Fig. 1).

3.3. Photoelectrochemical properties of Cu_2O films

The performances of the Cu_2O films were measured in terms of photocurrent through linear sweep voltammograms (Fig. 8) in 0.1 M Na_2SO_4–0.2 M acetate buffer solution (pH 4.9) under illumination with intensity of 35 mWcm^{-2}. The maximal output photocurrents for each of the electrodes, as measured from the respective LSV plots, are presented in Fig. 8 inset. It is evident that the photocurrent increases with a gradual addition of Eu(III) to the electrodeposition bath and reaches a maximum of 3.2 mA cm^{-2} at 2.5% Eu(III) concentration, beyond which it decreases again. The highest photocurrent observed for the Cu_2O film deposited from a solution containing 2.5% Eu(III) exceeds by 35–40% the photocurrent for the film obtained without Eu(III). Electrochemical behavior of the bare Eu-containing phases (i.e. film deposited from the said electrochemical bath in absence of Cu^{2+}) was evaluated through LSV under periodic illumination. Insignificant variation of current throughout the working potential range (as demonstrated by a nearly straight line plot in Fig. 8) indicates that the material reveals no PEC activity. The enhancement of photocurrent due to Eu(III) addition is observed also at higher intensity of incident light (100 mW cm^{-2} illumination, Fig. S2), although the photocurrent increases sublinearly with the light intensity.

Since we have not taken any measure to improve stability of the Eu modified Cu_2O films under illumination, the photocurrent demonstrated rather rapid decay (Fig. S3), which correlates with earlier experiments reported by other authors [59]. Stability of the semiconductor was tested through periodic voltammetry under chopped illumination (Fig. S3, inset), and it was found with the increase in the number of LSV pattern that the rate of photocurrent decrease is reduced after 2nd successive scans. Time instability of the photocurrent is contributed by the reduction of Cu_2O to metallic Cu, which was even visually observed through formation of black spots over the surface when the electrode was immersed in electrolytic media under illumination. SEM analysis of the sample prepared with optimized Eu(III) concentration after polarization studies indicates some specific changes of the surface morphology, as presented in Fig. S4a. The XRD pattern (Fig. S4b) shows reflexes at 43.7, 50.2 and 74.3° corresponding to elemental Cu, which also supports the above observations. Similar results were also reported in literature [13].

Fig. 9 presents the variation of IPCE for the Cu_2O films in 0.1 M Na_2SO_4 solution (pH 4.9 acetate buffer solution) when a fixed potential of 0.4 V vs. RHE was held. The maximal IPCE value of ~100% was recorded for the Cu_2O film deposited from electrolyte with 2.5% Eu(III) concentration, which can be considered as optimal, whereas the "pure" Cu_2O exhibits only 40% IPCE.

Since the Cu_2O films reveal a pronounced light scattering effect (Fig. S5a), we used IPCE instead transmittance spectra for determination of band gap energy E_g taking into account that IPCE is proportional to the absorption coefficient near the absorption edge. Another advance of using IPCE spectra is determined by minimization of impact of absorption mechanisms unrelated to PEC reactions [60,61]. As is seen from Fig. S5b, where the Tauc plots are given for direct allowed optical transitions, the variation of Eu(III) concentration in the electrodeposition bath has only slight impact on E_g indicating that the increase of photocurrent in the Eu-modified films is not related to E_g decrease, and suppression of charge carriers recombination is the most plausible reason of the observed effect.

One can see from Fig. 9 that the maximal enhancement of IPCE is attained for long wavelength light, when majority of electron-hole pairs are generated outside of the space charge region (SCR) and high lifetime values are required for participation of carriers in PEC reactions. However, the similar enhancement of IPCE due to Eu(III) addition to the electrodeposition bath is observed also for a short wavelength light, which is absorbed mainly in the thin near-surface part of film. Fig. 10

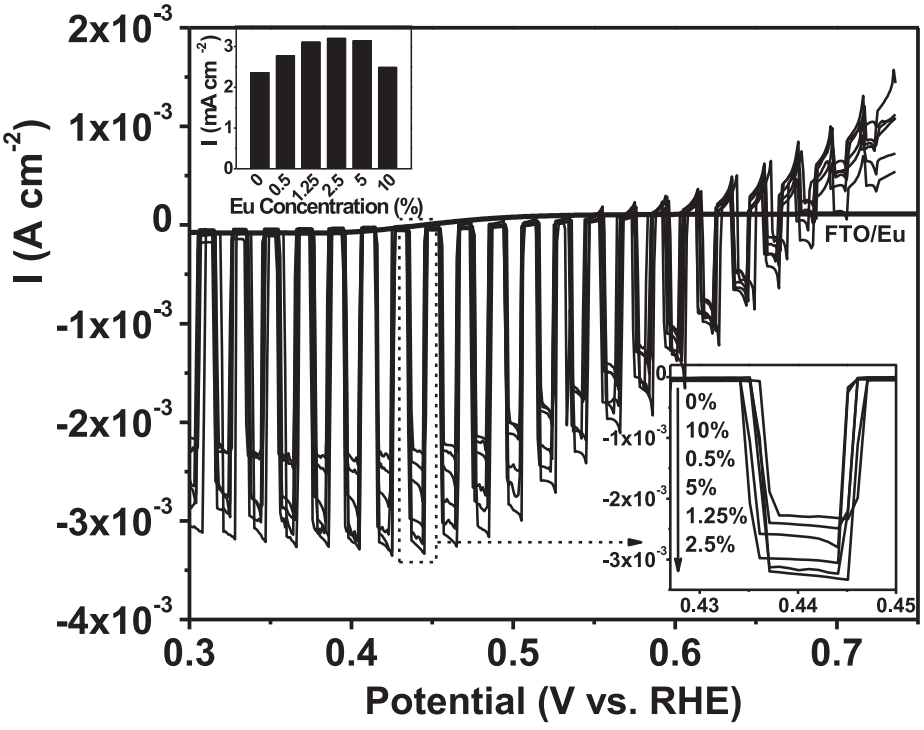

Fig. 8. LSV plots measured in pH4.9 acetate buffer solution under UV–visible illumination (Xe: 35 mW cm^{-2}) for Cu_2O films deposited from electrolytes with different Eu (III) concentrations; inset: variation of the maximal photocurrent with Eu(III) concentration in deposition electrolyte.

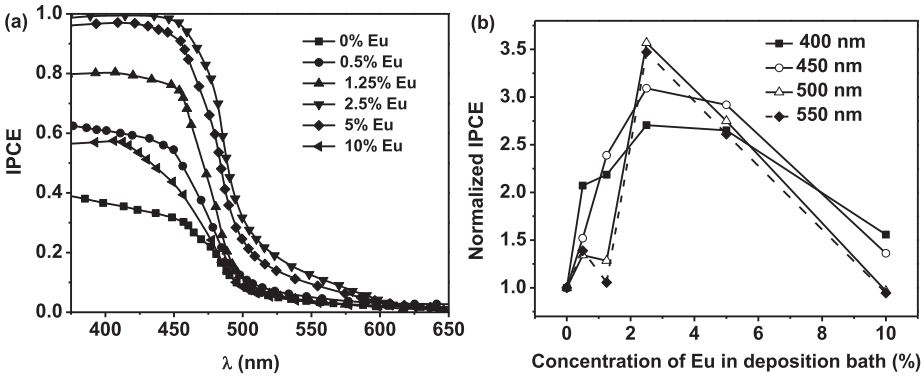

Fig. 9. (a) IPCE spectra for cathodic photocurrent for Cu_2O films deposited from electrolytes with different Eu(III) concentrations; (b) IPCE values derived from spectra presented in (a) and normalized to the corresponding values for the films grown without Eu(III) *vs* Eu(III) concentration in electrodeposition bath.

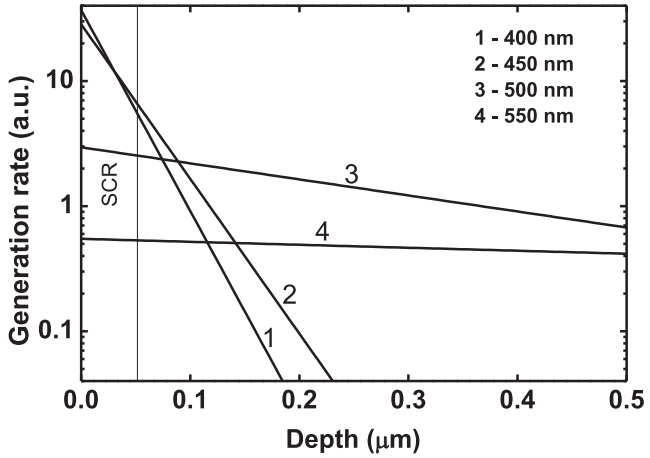

Fig. 10. Generation rate of electron-hole pairs depending on the depth for different wavelengths.

demonstrates in-depth profiles for generation rate of electron-hole pairs calculated using absorption coefficient values taken from [62]. The SCR width at potential of 0.4 V vs. RHE was estimated as $W_{scr} \approx 50$ nm from the Mott-Schottky plot (Fig. 7). In particular, for $\lambda = 400$ nm, 85% quanta are absorbed within the SCR. From this point of view, it seems strange that increase in lifetime of charge carriers influences remarkably on IPCE at this wavelength. To explain the afore-said contradiction, one should take into account that a conventional assumption about absence of recombination loss for the charge carriers generated within SCR is valid only if the following condition is true:

$$L_{dr} = \mu\tau E >> W_{scr}. \quad (1)$$

Here L_{dr} is the drift length of carriers, and μ and τ are their mobility and lifetime, respectively. According to the Poisson equation, the average electric field strength in SCR is

$$E = \frac{eN_A}{\varepsilon_0 \varepsilon} \frac{W_{SCR}}{2} \approx 2.7 \cdot 10^6 \, \mathrm{Vm}^{-1}. \quad (2)$$

Taking from [24] $\mu \approx 5 \, \mathrm{cm^2 \, V^{-1} \, s^{-1}}$ and $\tau \approx 90$ ps from our TCSPC experiments, we obtain $L_{dr} \approx 120$ nm, which is comparable with W_{SCR} and points to possibility of recombination of charge carriers generated within SCR.

Thus, the improved PEC performance of the Eu modified Cu_2O films over the pure material can be explained in the following way: (i) increase in size of the Cu_2O crystallites to some extent with a gradual addition of Eu(III) to the electrolytic bath leading to better coverage of the surface area and lowering of grain-boundary recombination; (ii) formation of a distinct Eu-containing precipitates which can act as gettering centers for detrimental impurities giving rise to purification of Cu_2O grains; (iii) this process in turn suppresses charge carrier recombination in the semiconductor matrix with increasing lifetime of the carriers; (iv) the photogenerated electrons in the conduction band therefore have more opportunity to participate in photoelectrochemical reduction of H_2O to generate H_2.

4. Conclusions

We have reported for the first time the electrodeposition of rare earth (Eu) modified *p*-type Cu_2O thin films. Presence of an optimized Eu (III) concentration in the electrodeposition bath (2.5% in respect to Cu (II) concentration) provides the highest photocurrent of 3.2 mA cm^{-2} (~100% quantum efficiency at $\lambda < 450$ nm) compared to 2.3 mA cm^{-2} for pure Cu_2O, measured at 0.4 V vs. RHE under 35 mW cm^{-2} illumination in the aqueous electrolyte (pH 4.9 buffer). XRD studies indicate single-phase composition of the films, whereas SEM-EDX analysis demonstrates the inclusions of Eu containing secondary phase on their surface. Electrochemical impedance Mott-Schottky analysis also indicates no change in bulk properties of all the Eu modified films, as their acceptor concentration and flat band potential remain invariant. The presence of Eu(III) in the bath influences the material in different ways such as an increased grain size with passivation of non-radiative recombination centers, which significantly enhance the photoluminescence emissions (by order of magnitude) through suppression of non-radiative recombination of the photogenerated charge carriers. Increase of carrier lifetime in the Eu modified films provides their improved photoelectrochemical properties compared to the pure Cu_2O.

Acknowledgments

The present work was financially supported by Board of Research in Nuclear Science (BRNS), Department of Atomic Energy (DAE) Govt. of India (File No. 2013/37C/61/BRNS). Financial assistance from DST International division for Indo-Belarus Joint Project (File no. DST/INT/BLR/P-7/2014), SERB-DST, Govt. of India (File no. SB/S1/PC-042/2013), DST, Govt. of West Bengal, (File no. 902(Sanc.)/ST/P/S & T/4G – 1/2013) and DST-FIST, Govt. of India (SR/FST/CSI-254/2013 for multifunctional time correlated single-photon counting (TCSPC) spectrophotometer) to the Department of Chemistry, IIEST, Shibpur are gratefully acknowledged. The work was also financially supported by the Research Programs “Photonics, Opto- and Microelectronics” (task 1.2.02) of the Republic of Belarus. We thank Dr. S.V. Gusakova and Dr. S.V. Zlotski for carrying out the SEM/EDX and XRD experiments, respectively. We also thank Dr. S. Ghosh of CSIR-CGCRI, Kolkata, India for carrying out XRD analysis of the polarized samples.

Appendix A. Supplementary data

Supplementary data associated with this article can be found, in the online version, at http://dx.doi.org/10.1016/j.cej.2017.11.004.

References

[1] A. Paracchino, V. Laporte, K. Sivula, M. Grätzel, E. Thimsen, Nat. Mater. 10 (2011) 456–461.
[2] X. An, K. Li, J. Tang, ChemSusChem 7 (2014) 1086–1093.
[3] A.D. Handoko, J. Tang, Int. J. Hydrogen Energy 38 (2013) 13017–13022.
[4] S.S. Jeong, A. Mittiga, E. Salza, A. Masci, S. Passerini, Electrochim. Acta 53 (2008) 2226–2231.
[5] P.E. de Jongh, D. Vanmaekelbergh, J.J. Kelly, Chem. Mater. 11 (1999) 3512–3517.
[6] K. Kardarian, D. Nunes, P.M. Sberna, A. Ginsburg, D.A. Keller, J.V. Pinto, J. Deuermeier, A.Y. Anderson, A. Zaban, R. Martins, E. Fortunato, Sol. Energy Mater. Sol. Cells 147 (2016) 27–36.
[7] A.E. Rakhshani, A.A. Al-Jassar, J. Varghese, Thin Solid Films 148 (1987) 191–201.
[8] A.E. Rakhshani, J. Varghese, Sol. Energy Mater. 15 (1987) 237–248.
[9] T.D. Golden, M.G. Shumsky, Y. Zhou, R.A. VanderWerf, R.A. Van Leeuwen, J.A. Switzer, Chem. Mater. 8 (1996) 2499–2504.
[10] P.E. de Jongh, D. Vanmaekelbergh, J.J. Kelly, J. Electrochem. Soc. 147 (2000) 486–489.
[11] T. Mahalingam, J.S.P. Chitra, S. Rajendran, M. Jayachandran, M.J. Chockalingam, J. Cryst. Growth 216 (2000) 304–310.
[12] W. Zhao, W. Fu, H. Yang, C. Tian, M. Li, Y. Li, L. Zhang, Y. Sui, X. Zhou, H. Chen, G. Zou, CrystEngComm 13 (2011) 2871–2877.
[13] A. Paracchino, J.C. Brauer, J.-E. Moser, E. Thimsen, M. Grätzel, J. Phys. Chem. C 116 (2012) 7341–7350.
[14] E.W. Bohannan, M.G. Shumsky, J.A. Switzer, Chem. Mater. 11 (1999) 2289–2291.
[15] R. Liu, E.W. Bohannan, J.A. Switzer, F. Oba, F. Ernst, Appl. Phys. Lett. 83 (2003) 1944–1946.
[16] R. Liu, F. Oba, E.W. Bohannan, F. Ernst, J.A. Switzer, Chem. Mater. 15 (2003) 4882–4885.
[17] J.A. Switzer, R. Liu, E.W. Bohannan, F. Ernst, J. Phys. Chem. B 106 (2002) 12369–12372.
[18] X. Liu, Y. Zhou, Appl. Phys. A 81 (2005) 685–689.
[19] J.-H. Zhong, G.-R. Li, Z.-L. Wang, Y.-N. Ou, Y.-X. Tong, Inorg. Chem. 50 (2011) 757–763.
[20] J. Luo, L. Steier, M.-K. Son, M. Schreier, M.T. Mayer, M. Grätzel, Nano Lett. 16 (2016) 1848–1857.
[21] Y.H. Lee, I.C. Leu, C.L. Liao, S.T. Chang, M.T. Wu, J.H. Yen, K.Z. Fung, Electrochem. Solid State Lett. 9 (2006) A207–A210.
[22] M.J. Siegfried, K.-S. Choi, Angew. Chem. 117 (2005) 3282–3287.
[23] C.J. Engel, T.A. Polson, J.R. Spado, J.M. Bell, A. Fillinger, J. Electrochem. Soc. 155 (2008) F37–F42.
[24] C.M. McShane, K.-S. Choi, J. Am. Chem. Soc. 131 (2009) 2561–2569.
[25] S. Bijani, M. Gabás, L. Martínez, J.R. Ramos-Barrado, J. Morales, Thin Solid Films 515 (2007) 5505–5511.
[26] M.J. Siegfried, K.-S. Choi, Angew. Chem. Int. Ed. 47 (2008) 368–372.
[27] L. Ma, Y. Lin, Y. Wang, J. Li, E. Wang, M. Qiu, Y. Yu, J. Phys. Chem. C 112 (2008) 18916–18922.
[28] J.N. Nian, C.C. Hu, H. Teng, Int. J. Hydrogen Energy 33 (2008) 2897–2903.
[29] A. Paracchino, N. Mathews, T. Hisatomi, M. Stefik, S. Tilley, M. Grätzel, Energy Environ. Sci. 5 (2012) 8673–8681.
[30] L.C. Wang, N.R. de Tacconi, C.R. Chenthamarakshan, K. Rajeshwar, M. Tao, Thin Solid Films 515 (2007) 3090–3095.
[31] L. Wang, M. Tao, Electrochem. Solid-State Lett. 10 (2007) H248–H250.
[32] K. Han, M. Tao, Sol. Energy Mater. Sol. Cells 93 (2009) 153–157.
[33] C. Zhu, M.J. Panzer, A.C.S. Appl, Mater. Interfaces 7 (2015) 5624–5628.
[34] C.M. McShane, W.P. Siripala, K.-S. Choi, J. Phys. Chem. Lett. 1 (2010) 2666–2670.
[35] S. Shyamal, P. Hajra, H. Mandal, J.K. Singh, A.K. Satpati, S. Pande, C. Bhattacharya, A.C.S. Appl, Mater. Interfaces 7 (2015) 18344–18352.
[36] S. Shyamal, P. Hajra, H. Mandal, A. Bera, D. Sariket, A.K. Satpati, S. Kundu, C. Bhattacharya, J. Mater. Chem. A 4 (2016) 9244–9252.
[37] K. Mizuno, M. Izaki, K. Murase, T. Shinagawa, M. Chigane, M. Inaba, A. Tasaka, Y. Awakura, J. Electrochem. Soc. 152 (2005) C179–C182.
[38] L. Wu, L.-k Tsui, N. Swami, G. Zangari, J. Phys. Chem. C 114 (2010) 11551–11556.
[39] M. Pourbaix Atlas of Electrochemical Equilibria in Aqueous Solutions, 2nd English ed. 1974 Houston National Association of Corrosion Engineers 384.
[40] Z. Zang, A. Nakamura, J. Temmyo, Optics Express 21 (2013) 11448–11454.
[41] Z. Zang, A. Nakamura, J. Temmyo, Mater. Lett. 92 (2013) 188–191.
[42] D. Gilles, E.R. Weber, S.K. Hahn, Phys. Rev. Lett. 64 (1990) 196–199.
[43] A.Y. Liu, C. Sun, V.P. Markevich, A.R. Peaker, J.D. Murphy, D. Macdonald, J. Appl. Phys. 120 (2016) 193103–193110.
[44] W.M. Haynes (Ed.). CRC Handbook of Chemistry and Physics, 96th ed., Boca Raton, 2015-16.
[45] Atlas of E-pH diagrams, Geological Survey of Japan Open File Report No.419, Naoto TAKENO, May 2005.
[46] P.F. Williams, S.P.S. Porto, Phys. Rev. B 8 (1973) 1782–1785.
[47] H. Hagemann, H. Bill, W. Sadowski, E.M. Walker, Solid State Commun. 73 (1990) 447–451.
[48] J.-G. Kang, Y. Jung, B.-K. Min, Y. Sohn, Appl. Surf. Sci. 314 (2014) 158–165.
[49] J.C. Hamilton, J.C. Farmer, R.J. Anderson, J. Electrochem. Soc. 133 (1986) 739–745.
[50] K. Reimann, K. Syassen, Phys. Rev. B 39 (1989) 11113.
[51] T. Sander, C.T. Reindl, M. Giar, B. Eifert, M. Heinemann, C. Heiliger, P.J. Klar, Phys. Rev. B 90 (2014) 045203.
[52] M.C. Biesinger, L.W.M. Lau, A.R. Gerson, R. St, C. Smart, Appl. Surf. Sci. 257 (2010) 887–898.
[53] D. Li, X. Zhang, L. Jin, D. Yang, Opt. Express 18 (2010) 27191–27196.
[54] Y. Wang, S. Li, H. Shi, K. Yu, Nanoscale 4 (2012) 7817–7824.
[55] E.F. Gross, N.A. Karryjew, Dokl. Akad. Nauk SSSR 84 (1952) 471–474.
[56] V. Grivickas, K. Gulbinas, V. Gavryushin, V. Bikbajevas, O.V. Korolik, A.V. Mazanik, A.K. Fedotov, Phys. Status Solidi RRL 8 (2014) 639–642.
[57] A.J. Bard, L.R. Faulkner, Electrochemical Methods Fundamentals and Application, second ed., John Wiley & Sons, New York, 2001.
[58] F. Pei, S. Wu, G. Wang, M. Xu, Y.S. Wang, L. Chen, J. Korean Phys. Soc. 55 (2009) 1243–1249.
[59] C. Li, Y. Li, J.J. Delaunay, A.C.S. Appl, Mater. Interfaces 6 (2014) 480–486.
[60] E.A. Bondarenko, E.A. Streltsov, M.V. Malashchonak, A.V. Mazanik, A.I. Kulak, E.V. Skorb, Adv. Mater. (2017), http://dx.doi.org/10.1002/adma.201702387.
[61] M.V. Malashchonak, E.A. Streltsov, D.A. Kuliomin, A.I. Kulak, A.V. Mazanik, Mater. Chem. Phys. 201 (2017) 189–193.
[62] C. Malerba, F. Biccari, C.L.A. Ricardo, M. D'Incau, P. Scardi, A. Mittiga, Sol. Energy Mater. Sol. Cells 95 (2011) 2848–2854.